

# Conformal Wide-Angle Scanning Leaky-Wave Antenna for V-Band On-Body Applications

Pratik Vadher, *Student Member, IEEE*, Anja K. Skrivervik, Qihang Zeng, *Member, IEEE*, Ronan Sauleau, *Fellow, IEEE*, John S. Ho, *Member, IEEE*, Giulia Sacco, *Member, IEEE*, and Denys Nikolayev, *Senior Member, IEEE*

**Abstract**—Wearable on-body millimeter-wave (mmWave) radars can provide obstacle detection and guidance for visually impaired people. However, their everyday performance is hindered by the rigid form factor and limited scanning range. In this article, we propose a low-profile, fast-scanning leaky-wave antenna (LWA) operating in the unlicensed V-band (57–64 GHz) to be integrated for on-body applications such as lightweight portable frequency-modulated continuous wave (FMCW) radars. The proposed LWA consists of meandering microstrips that can conform to the human body curvatures while maintaining beam-forming and beam-scanning properties. Experimental results demonstrate that the planar LWA achieves a realized gain above 10 dB with a fan-beam steering range in the H-plane from  $-40^\circ$  to  $43^\circ$  over the operating frequency band while the half power beam-width (HPBW) is within  $20^\circ$ . Since for the foreseen application the antenna is supposed to conform to the user's body, the performance is also analyzed for a bent condition. The beam steering range changes to  $-32^\circ$  to  $50^\circ$  when placed on the knee (corresponding to 80 mm radius). Under bending conditions, the LWA exhibits a maximum degradation of 1.75 dB, while the HPBW increases to  $25^\circ$ . This shows that due to the small size of the antenna, the impact of bending is low and the beam-forming and beam-scanning property of the designed LWA remain intact. Furthermore, we enable 2-D spatial scanning by employing an array of twelve LWAs with phased excitation, extending the scanning range in the E-plane from  $-40^\circ$  to  $40^\circ$ , while the HPBW remains below  $20^\circ$  across the operational frequency range.

**Index Terms**—leaky-wave antenna (LWA), wearable radars, V-band, higher spatial order, meandering microstrip antenna, conformal antenna.

## I. INTRODUCTION

Enhancing navigation aids for visually impaired people is essential for improving their mobility and independence.

Manuscript received July XX, 2024, revised XX X, 2024.

This project has received funding from the French Agence Nationale de la Recherche (ANR) through the Project MedWave under Grant ANR-21-CE19-0045; and by the European Union's Horizon Europe research and innovation program through the Marie Skłodowska-Curie INSIGHT project N°101063966. (*Corresponding authors: Denys Nikolayev, denys.nikolayev@deniq.com; Giulia Sacco, giulia.sacco@univ-rennes1.fr*)

This work is supported by the European Union through European Regional Development Fund (ERDF), Ministry of Higher Education and Research, CNRS, Brittany region, Conseils Départementaux d'Ille-et-Vilaine and Côtes d'Armor, Rennes Métropole, and Lannion Trégor Communauté, through the CPER Project CyMoCod.

P. Vadher, R. Sauleau, G. Sacco, and D. Nikolayev are with the IETR – UMR 6164, CNRS / Univ Rennes, FR-35000 Rennes, France.

A. K. Skrivervik is with the Microwave and Antenna Group, Ecole Polytechnique Fédérale de Lausanne, CH-1015 Lausanne, Switzerland.

Q. Zeng, and J. S. Ho are with the Department of Electrical and Computer Engineering, the Institute for Health Innovation and Technology, and the N.1 Institute, National University of Singapore, Singapore 117583

Recent advancements in mobile technology have led to an increased interest in developing wearable devices as assistive tools for individuals with visual impairments [1–4]. Of the various sensing modalities, millimeter-wave (mmWave) radars offer a cost-effective, lightweight, and robust sensing solution, since they do not depend on the ambient light conditions and do not affect the user's privacy. In particular, short range frequency-modulated continuous wave (FMCW) radars can be implemented in a compact electronic system due to their low power consumption and low profile [1], [5]. Traditionally these sensors have been placed on rigid objects (e.g., white canes and engineered glasses) which can burden the user [1], [6]. An improved solution consists in placing the radar on the user's body in a way that does not hamper their movements, and that is comfortable to be worn [7].

To facilitate radar-based sensing within a wearable form factor, unlicensed V-band extending from 57 GHz to 64 GHz is a promising solution for radar applications, since it provides a high range resolution, while being less susceptible to the interference from nearby devices [8]. A compact radar can be implemented with a low profile unobtrusive conformal antenna. When positioning the antenna on the user's body, the compact size of the conformal antenna at these frequencies, reduces the impact of body curvature (radius ranging from 40 mm to 240 mm [9]) by limiting the bending-related distortions.

Leaky-wave antennas (LWAs) can be fed very easily and provide main-beam steering capability with frequency due to the dispersive nature of the guiding media [10–12]. Since the antenna is to be placed conformally on the user's body, it is of paramount importance that the antenna is flexible [13], [14]. To improve flexibility and reduce manufacturing costs, microstrip-based LWAs [15–18] are preferable to substrate integrated waveguide (SIW) based LWAs [19–21] given the absence of via holes. Additionally, periodic meandering microstrips LWAs provide a good control over the path taken by the electromagnetic (EM) wave in the guiding medium, since the microstrip intervals between the corners—corresponding to the radiating discontinuities in this type of LWA—can be tailored to ensure optimal polarization and scanning range of the main fan-beam [15], [22], [23].

For radar applications where localization is required, it is advisable to have large angular coverage [5], [24]. To fulfill this purpose, the use of LWA in combination with FMCW radars represents a promising solution to limit the number of channels and the use of complex phase shifters [25], [26].

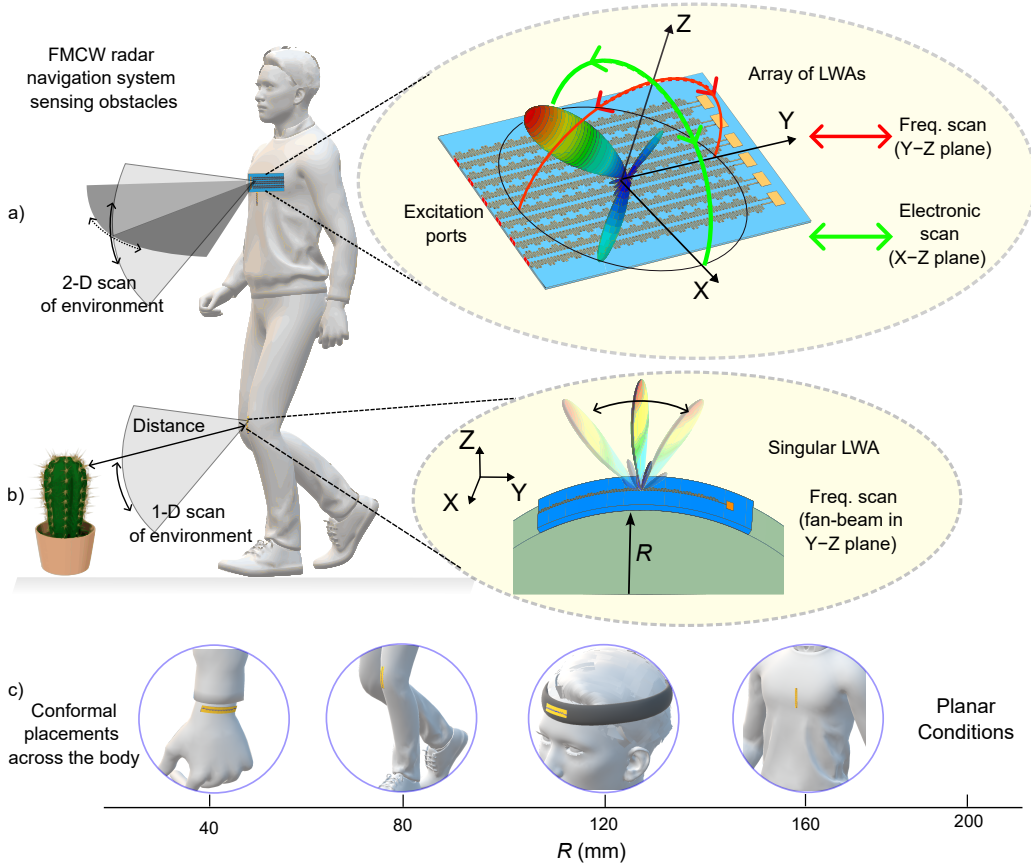


Fig. 1: An on-body FMCW V-band radar for sensing and detecting obstacles in the outdoor environment. (a) Array of 12 LWAs. The scan in the Y-Z plane is due to frequency scanning, while the scanning in X-Z plane is due to electronic scanning. (b) A single LWA and radiated fan-beam in the Y-Z plane. (c) Possible antenna placements and corresponding curvature radii.

LWAs proposed earlier for such applications in V-band [16], [24] can have large scanning range, but are characterized by a low rate of change of the main beam pointing direction with frequency, i.e., a low beam steering rate ( $S_m$ ). To limit the spectral resources for a given scanning range [11], [27], [28], a faster  $S_m$  is required.

Here we propose and demonstrate a conformal LWA that can be fabricated using a single printed layer and provides wide-scanning angle from  $-40^\circ$  to  $43^\circ$  and  $-32^\circ$  to  $50^\circ$  when deformed on a curved surface over the operating range. The unit cell is composed of 4 meanders. The microstrip-based design of the LWA provides an effective control over the size of unit cell and hence over  $S_m$ . The length of the microstrip intervals between the mitred corners (radiating discontinuities) are tailored to improve cross-polarization discrimination (XPD) ratio over a wide operation band 57 GHz to 64 GHz.

The paper is structured as follows. Section II describes the proposed antenna system and conformal wearable implementations. Section III explains the leaky-wave theory of the proposed antenna followed by the construction of a meandered guiding medium resulting in a slow wave structure (SWS). A technique to modify the SWS to obtain a radiation, while eliminating the open stopband (OSB) is subsequently explained. Section IV describes the design of feeding structure and the measurements of the designed prototype in planar and conformal environments. Section V contains the comparison

with state-of-the-art followed by conclusions.

## II. OPERATIONAL PRINCIPLE AND ANTENNA REQUIREMENTS

A lightweight wearable on-body radar should be able to detect and warn users of obstacles, as well as create a map of their surroundings to aid their navigation [Fig. 1 (a,b)]. The proposed antenna system is designed to be used in combination with an FMCW radar. To enable the 2-D scanning, an array of twelve LWAs is used as shown in Fig. 1(a). The scanning in the Y-Z plane is ensured by the leaky-wave phenomenon, while the beamforming in the X-Z plane is obtained electronically, by modifying the excitation of the different LWAs [29], [30]. Furthermore, the antenna can be positioned conformally to the body surface, as shown in the Fig. 1(b). Some possible locations along with the typical curvature radii [9] are shown in Fig. 1(c). The LWA is backed by a ground plane to limit the radiation towards the user [16].

## III. LEAKY-WAVE THEORY FOR THE PROPOSED ANTENNA

Fig. 2 shows the design of the proposed periodic meandering microstrip based LWA. A 0.254 mm-thick layer of Rogers 3003 ( $\epsilon_r = 3.0$ ,  $\tan \delta = 0.0010$ ) is utilised as substrate. The structure leaks energy due to the mitred corners which act as radiating discontinuities. The leaky radiation due to a periodic structure can be analyzed by the Bloch-Floquet



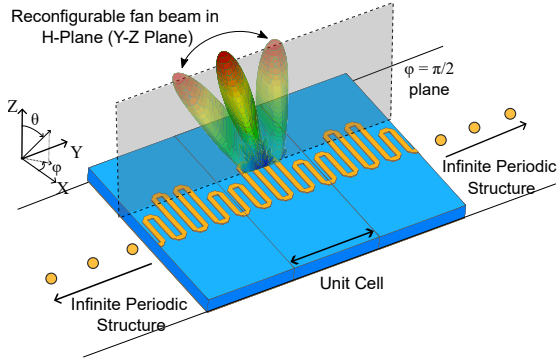


Fig. 2: Conductor backed periodic meandering microstrip LWA.

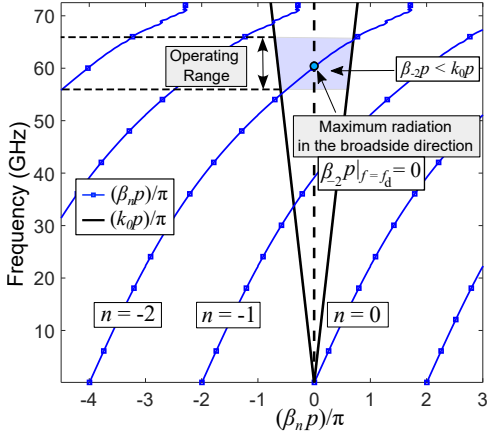


Fig. 3: Brillouin diagram of the proposed leaky-wave meandering microstrip structure.

theorem with the use of spatial harmonics [31], [32]. The phase constant corresponding to the  $n^{\text{th}}$  space harmonic  $\beta_n$  satisfies

$$\beta_n p = \beta_0 p + 2n\pi, \quad (1)$$

where  $n$  ranges from  $-\infty$  to  $+\infty$ . Here  $\beta_0$  is the zeroth order spatial harmonic of a periodic LWA.

The spatial harmonics that satisfy the condition  $|\beta_n|p < |k_0|p$  contribute to the leaky-wave radiation. A guiding medium with periodic radiating discontinuities can scan the main beam from backward to forward direction.

If most of the power from the structure is radiated, the direction of maximum radiation  $\theta_{max,n}$  corresponding to the  $n^{\text{th}}$  spatial harmonic is given by [32-35]

$$\theta_{max,n} = \sin^{-1}(\beta_{-n} p / k_0 p), \quad (2)$$

where  $k_0$  is the free space wave number.

For the proposed structure, the  $n = -2$  spatial harmonic, as shown in the Brillouin diagram in Fig. 3, is responsible for radiation in desired operating range (57 GHz–64 GHz).

Consequently, according to equation (2), when the phase difference across the unit cell ( $\beta_{-n} p$ ) is zero, the direction of the main beam associated to the  $n^{\text{th}}$  spatial harmonic is broadside. Since the spatial harmonic  $n = -2$  is responsible for radiation in the desired band, the phase difference across the unit cell with a period  $p$  from equation (1) corresponds to:

$$\beta_{-2} p |_{f=f_d} = 0 \rightarrow \beta_0 p |_{f=f_d} = 4\pi, \quad (3)$$

where  $f_d$  is the desired frequency corresponding to the broadside radiation for  $n = -2$ . Equation (3) further implies that  $\beta_{0,tem} |_{f=f_d} \times l = 4\pi$  [15], [22]. Here,  $\beta_{0,tem}$  is the phase constant of the microstrip media,  $l$  denotes the total pathlength of the meandering microstrips. The pathlength of the microstrip is calculated based on the model proposed by [23].

#### A. Non-radiating Guiding Medium with Dispersion Control

A meandering microstrip structure with equal meanders is shown in Fig. 4 (depicted as solid boundary line). The phase contributions corresponding to the horizontal and vertical intervals of the meander are listed in Table I. A guiding medium based on meandering microstrip allows to finely control the path of the travelling wave by altering the length of the intervals between the corners of the meander [36].

The proposed SWS is designed such that a single meander results in a phase difference of  $\pi$  at  $f_d$ . The rate of change of the phase constant ( $\beta$ ) with frequency (i.e., the dispersion rate) can be increased by decreasing the period  $p_0$  of the single meander. The period  $p_0$  can be reduced—while maintaining the same electrical length of the meander—by decreasing the horizontal interval and increasing the vertical interval of the meander by the same amount. Consequently, the impact of the variation of the horizontal segment (denoted by  $\zeta$ ) on  $\beta$  is shown in Fig.5a indicating a high control over the dispersion rate of the meandering microstrip guiding medium.

In the desired operating range of 57 to 64 GHz, the dispersion constant of the structure lies outside the light cone, resulting in a confined surface wave within the guiding medium without any leaky radiation. This is illustrated in Fig. 5b, which shows the magnitude of the E-field obtained from the full-wave simulation of 72 cascaded meanders (equivalent to the final length of the LWA), all having equal lengths with  $\zeta = \pi/15$  and  $\Delta\psi = 0$  at  $f_d$ .

#### B. Meandered LWA

The radiation resulting from a microstrip based LWA can be analysed in terms of residual magnetic current densities ( $\mathcal{J}_m$ ) at the corners [22], [37]. The residual currents at each corner are shown in Fig. 4. To achieve constructive addition of the electric fields from the residual currents, the vertical length of the meanders can be periodically varied.

To obtain a periodic unit cell, four meanders designed in the previous section are cascaded in series [Fig.4]. It is possible to modify the vertical length of the meanders without changing the total pathlength of the unit cell ( $4\pi$  for four meanders at  $f_d$ ) to obtain a radiation in the far-field at  $f_d$ . This is achieved by decreasing the vertical length of the first meander by  $\Delta x$ , and increasing the length of the second meander by the same quantity. A length  $\Delta x$  results in a phase delay of  $\Delta\psi$  at  $f_d$  (Table I). The third and fourth meanders are modified accordingly to obtain a symmetric unit cell. The resultant unit cell is depicted as grey in the Fig.4

For the proposed unit cell, the corners are denominated by  $L_{i,n}$ ,  $L^a_{i,n}$ ,  $R^a_{i,n}$ , and  $R_{i,n}$ , where  $i \in \{1, 2, 3, 4\}$  indicates the  $i^{\text{th}}$

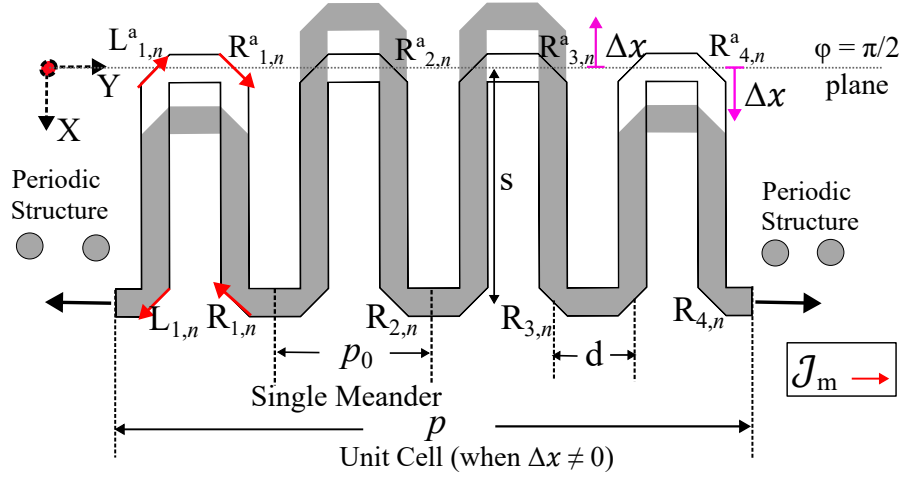


Fig. 4: Meandered microstrip guiding medium with equal meanders (shown as solid line) behaving as non-radiating slow-wave structure; and unit cell formed by 4 modulated meanders (shown in grey) for constructive radiation leading to leaky-wave behaviour.

TABLE I: Geometrical parameters (Fig. 4) and corresponding phase differences at the design frequency  $f_d$ .

Segment	Denoted by	Phase diff. at $f_d$	Prototyped Dimensions	
			(rad)	(mm)
Horizontal length of meander	$d$	$\zeta$	$\pi/15$	0.11
Vertical length of meander	$s$	$\pi/2 - \zeta$	$\pi/2 - \pi/15$	0.868
Change in vertical length of meander	$\Delta x$	$\Delta\psi$	0.3	0.158

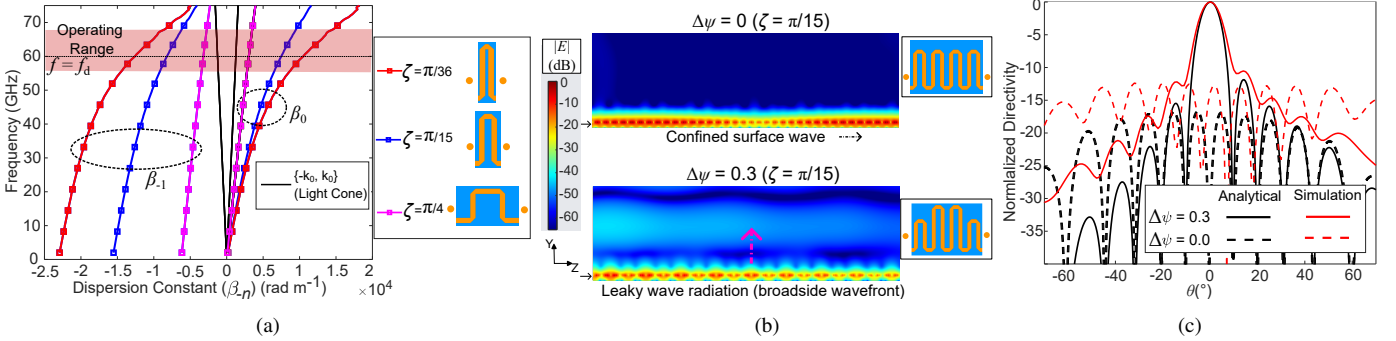


Fig. 5: (a) Phase constant vs frequency for a structure with equal meanders (b) Distribution of the absolute value of the  $\mathbf{E}$  field in the H-Plane (Y-Z Plane). Confined surface waves at  $f_d$  for a structure with equal meanders ( $\Delta\psi = 0$ ) and leaky-wave radiation for the case  $\Delta\psi = 0.3$  as the wave travels down the meandering microstrips, (c) Changes in the directivity of the proposed structure at  $f_d$  (in the broadside radiation) for two cases of  $\Delta\psi$  (for  $\zeta = \pi/15$ ).

TABLE II: Phase shifts of  $\mathbf{E}$  at the mitred corners corresponding to  $R_{i,1}$  and  $R^a_{i,1}$  at  $f_d$  induced by the pathlength.

Corner	$R^a_{1,1}$	$R_{1,1}$	$R^a_{2,1}$	$R_{2,1}$	$R^a_{3,1}$	$R_{3,1}$	$R^a_{4,1}$	$R_{4,1}$
Spatial Vector Direction	$(\hat{x} + \hat{y})$	$(-\hat{x} - \hat{y})$	$(\hat{x} + \hat{y})$	$(-\hat{x} - \hat{y})$	$(\hat{x} + \hat{y})$	$(-\hat{x} - \hat{y})$	$(\hat{x} + \hat{y})$	$(-\hat{x} - \hat{y})$
Phase at $f_d$	$\frac{\pi}{2} + \frac{\zeta}{2} - \Delta\psi$	$\pi - \frac{\zeta}{2} - 2\Delta\psi$	$\frac{3\pi}{2} + \frac{\zeta}{2} + \Delta\psi$	$2\pi - \frac{\zeta}{2}$	$\frac{5\pi}{2} + \frac{\zeta}{2} + \Delta\psi$	$3\pi - \frac{\zeta}{2} + 2\Delta\psi$	$\frac{7\pi}{2} + \frac{\zeta}{2} + \Delta\psi$	$4\pi - \frac{\zeta}{2}$

TABLE III: Phase shifts of  $\mathbf{E}$  at the mitred corners corresponding to  $L_{i,1}$  and  $L^a_{i,1}$  at  $f_d$  induced by the pathlength.

Corner	$L^a_{1,1}$	$L_{1,1}$	$L^a_{2,1}$	$L_{2,1}$	$L^a_{3,1}$	$L_{3,1}$	$L^a_{4,1}$	$L_{4,1}$
Spatial Vector Direction	$(-\hat{x} + \hat{y})$	$(\hat{x} - \hat{y})$	$(-\hat{x} + \hat{y})$	$(\hat{x} - \hat{y})$	$(-\hat{x} + \hat{y})$	$(\hat{x} - \hat{y})$	$(-\hat{x} + \hat{y})$	$(\hat{x} - \hat{y})$
Phase at $f_d$	$\frac{\pi}{2} - \frac{\zeta}{2} - \Delta\psi$	$\frac{\zeta}{2}$	$\frac{3\pi}{2} - \frac{\zeta}{2} + \Delta\psi$	$\pi + \frac{\zeta}{2} + 2\Delta\psi$	$\frac{5\pi}{2} - \frac{\zeta}{2} + \Delta\psi$	$2\pi + \frac{\zeta}{2}$	$\frac{7\pi}{2} - \frac{\zeta}{2} + \Delta\psi$	$3\pi + \frac{\zeta}{2} + 2\Delta\psi$

meander within the unit cell, and  $n \in [1, N]$  corresponds to the  $n^{\text{th}}$  unit cell,  $N$  being the total number of unit cells (Fig.4).

The microstrip line intervals result in a phase delay between the corners. The phases corresponding to the corners of the first unit cell are indicated in Table II and Table III.

Since equation (3) is satisfied at  $f_d$ —the radiation occurs in the broadside direction. Subsequently, the ratio of the total electric field generated by  $N$  such unit cells is obtained as the summation of the electric fields for the unit cell [38] shown in Fig.4 generated by the  $\mathcal{J}_m$  oriented towards the direction  $(+\hat{x} + \hat{y})$  is:

$$\frac{E_{R_{2,n}^a|f=f_d}^{\text{tot}}}{E_{R_{1,n}^a|f=f_d}^{\text{tot}}} = \frac{\sum_{n=1}^N e^{-j(\frac{3\pi}{2} + \frac{\zeta}{2} - \Delta\psi + 4(n-1)\pi)}}{\sum_{n=1}^N e^{-j(\frac{\pi}{2} + \frac{\zeta}{2} - \Delta\psi + 4(n-1)\pi)}} = -1 \quad (4)$$

$$\frac{E_{R_{4,n}^a|f=f_d}^{\text{tot}}}{E_{R_{3,n}^a|f=f_d}^{\text{tot}}} = \frac{\sum_{n=1}^N e^{-j(\frac{7\pi}{2} + \frac{\zeta}{2} + \Delta\psi + 4(n-1)\pi)}}{\sum_{n=1}^N e^{-j(\frac{5\pi}{2} + \frac{\zeta}{2} + \Delta\psi + 4(n-1)\pi)}} = -1 \quad (5)$$

The ratio of the total electric field generated by the summation of the contributions  $\mathcal{J}_m$  oriented towards the direction  $(-\hat{x} - \hat{y})$  at  $f_d$  corresponds to:

$$\frac{E_{R_{2,n}^b|f=f_d}^{\text{tot}}}{E_{R_{1,n}^b|f=f_d}^{\text{tot}}} = \frac{\sum_{n=1}^N e^{-j(2\pi - \frac{\zeta}{2} + 4(n-1)\pi)}}{\sum_{n=1}^N e^{-j(\pi - \frac{\zeta}{2} - 2\Delta\psi + 4(n-1)\pi)}} = -e^{-2j\Delta\psi} \quad (6)$$

$$\frac{E_{R_{4,n}^b|f=f_d}^{\text{tot}}}{E_{R_{3,n}^b|f=f_d}^{\text{tot}}} = \frac{\sum_{n=1}^N e^{-j(4\pi - \frac{\zeta}{2} + 4(n-1)\pi)}}{\sum_{n=1}^N e^{-j(3\pi - \frac{\zeta}{2} + 2\Delta\psi + 4(n-1)\pi)}} = -e^{2j\Delta\psi} \quad (7)$$

Equations (4) and (5) show that the electric fields at the corners  $R_{i,n}^a$  are opposite to each other, while the electric field vectors at  $R_{i,n}$  ( $i \in [1, 4]$ ) contribute to the far-field. By repeating the same analysis for the corners  $L_{i,n}$  and  $L_{i,n}^a$  (the phase at these are indicated in Table III) it is possible to derive the same conclusion.

Note that if  $\Delta\psi = 0$ , the resultant electric field is zero, reducing the structure to the non-radiating SWS shown in Fig. 4 (equal meanders, depicted as solid line).

An analytical model based on the equations is created to verify the effectiveness and the results are compared with full-wave-simulations as shown in Fig. 5c at  $f_d$ . As can be observed, when  $\Delta\psi = 0$ , all the meanders are of equal size leading to no radiation, when the meanders become unequal with  $\Delta\psi = 0.3$ , there is radiation. The above model adopts simplifying assumptions, treating radiation sources as magnetic line currents at the corners, as proposed by [23], [39]. Additionally, it assumes that the attenuation of the traveling wave down the line is minimal and that the bends are matched, resulting in no reflections. Although this approach [40] loses information about mutual coupling, the effect of OSB and substrate surface waves, it offers closed-form design solutions to guide the design of the proposed meandering-microstrip LWA for the desirable radiation characteristics at the frequency of broadside radiation.

### C. OSB Mitigation

A periodic structure has stop-bands, that result in a very low transmission of the wave through the structure and in high energy being reflected back to the source in this band of frequencies [31]. OSB occurring inside the radiation zone limits the scanning near the the broadside direction [31], [41] and needs to be mitigated.

The Bloch impedance  $Z_s$  can be used to characterize the presence of OSB [42]. The  $Z_s$  can be calculated from the ABCD-parameters obtained from the S-parameters computed in full-wave simulations [43]:

$$Z_s = \frac{-2 \times B}{(A - D - \sqrt{(A + D)^2 - 4})}. \quad (8)$$

Fig. 6a indicates that there is a resonance in the band around  $f_d$  contributing to OSB. The impact of OSB on the antenna performance in terms of realized gain of the LWA is shown in Fig. 6b. There is a severe reduction in gain in the broadside direction if OSB is not mitigated.

Asymmetry can be introduced in the unit cell to mitigate OSB as shown in [15], [44] and [45]. Changing the angles of corners of the final two meanders as shown in the Fig.6c introduces a small phase shift between the first couple and the second couple meanders to avoid strong resonance and large reflection in the band around  $f_d$ . OSB mitigation can be observed from the Bloch impedance  $Z_s$  plot with frequency [see Fig. 6a]. For  $\zeta = \pi/15$  and  $\Delta\psi = 0.3$ , a value of  $\delta q$  equal to 0.05 mm is selected. The increase in the realized gain can be observed at the broadside direction in Fig. 6a. Additionally, it can be noted that, since at  $f_d$  the contribution to the far-field is not provided by the corners  $L_{i,n}^a$  and  $R_{i,n}^a$ , the change in the angle of these corners will not affect the fields radiated from the contributing corners  $L_{i,n}$  and  $R_{i,n}$ .

Following the mitigation of OSB, the maximum realized gain obtained at the broadside frequency as a function of  $\Delta\psi$  is depicted in Fig.7 with  $N = 30$  unit cells for  $\zeta = \pi/15$ .

### D. Impact of $\Delta\psi$ in the Operating Band

Full-wave simulations with  $N = 30$  unit cells have been performed to quantify the impact of  $\Delta\psi$  on the LWA far-field in the band of operation (57–64 GHz) after the mitigation of OSB.

Fig.8a shows the change in realized gain for different values of  $\Delta\psi$  with  $\zeta = \pi/15$ . Figures 7 and 8a show that the realized gain initially increases with an increase in  $\Delta\psi$ , but then levels off after certain value of  $\Delta\psi$  ( $= 0.3$  in the current case). This indicates that the unit cell becomes a more effective radiator as  $\Delta\psi$  increases up to this point. As the radiation from each unit cell increases, the effective aperture of the LWA reduces, resulting in larger 3-dB beamwidth as indicated in the Fig.8b.

As indicated earlier, for a frequency scanning antenna of an FMCW radar, the three parameters scanning rate, realized gain and 3-dB beamwidth are important [11], [46]. In the proposed LWA,  $\zeta$  can be varied to control the scanning rate and hence the angular scanning of the antenna.  $\Delta\psi$  can be then be increased to obtain desired realized gain and beamwidth values. For the current prototype, the chosen parameters are

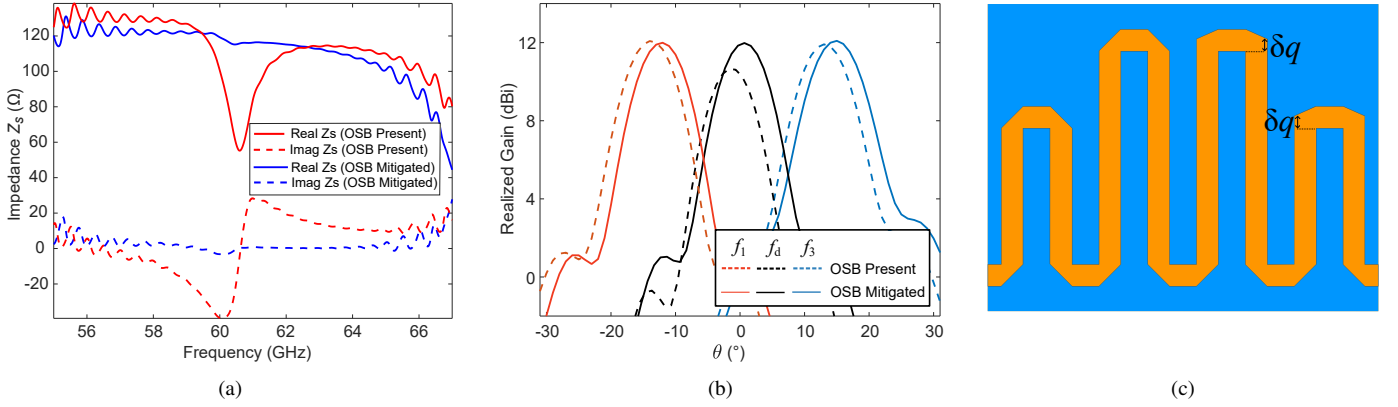


Fig. 6: (a) Bloch impedance  $Z_s$  vs frequency, (b) Impact on the realized gain before and after removal of OSB at the frequency  $f_d$  in the broadside direction. Here,  $f_1 = f_d - 1$  GHz and  $f_2 = f_d + 1$  GHz. (c) Removal of OSB by changing the angle of mitred corner for the third and fourth meander of the unit cell.

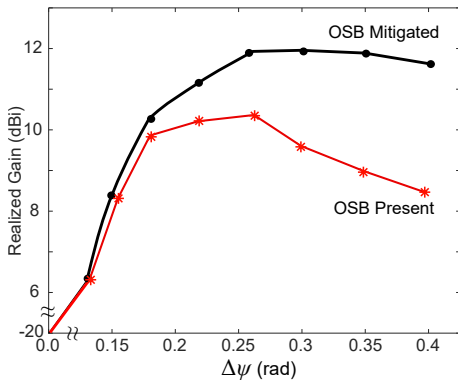


Fig. 7: Realized gain at  $f_d$  (in the broadside radiation) as a function of  $\Delta\psi$  (for  $\zeta = \pi/15$ ).

listed in Table I which result in realized gain of 10 dB and angular scanning of  $80^\circ$  symmetrically through broadside and across the operating band.

### E. Impact of the Number of Unit Cells

To maximise the radiation efficiency and radiate most of the energy from the leaky-wave structure, while keeping it compact, determining the number of unit cells to be included in the final design is of the utmost importance. Fig. 8c shows the change in gain with the increase in the number of unit cells. After  $N = 18$  unit cells, the change in gain is minimal.

Further increasing the number of unit cells would result in a reduction of the radiation efficiency as well as in an increase of the antenna dimensions. It is worth noticing that the performance of a longer antenna is more likely to be impacted by the bending. Hence  $N = 18$  unit cells is set as the optimal length.

## IV. PROTOTYPE AND MEASUREMENTS FOR THE PROPOSED ANTENNA

### A. Design of the Feed

The designed LWA based on a conductor-backed meandering microstrip is fed *via* a 1.85 mm end-launch Southwest connector. The feed is designed to avoid the use of vias in the transition from connector (coaxial) to microstrip. Hence a

TABLE IV  
DIMENSIONS OF THE FEED AND THE TERMINATING PATCH.

Dimensions	Physical dim. (mm)
Co <sub>SL</sub>	2.8
Co <sub>T</sub>	1.5
Co <sub>G</sub>	2.47
Co <sub>L</sub>	1.75
t <sub>50</sub>	0.69
Tx	2.5
W <sub>patch</sub>	2.55
L <sub>patch</sub>	1.23

conductor-backed co-planar waveguide transition is used as shown in the Fig. 9a. This is done to avoid the spurious radiation occurring during the transition from co-axial feed to the microstrip. The feed is designed to provide optimal performance in the antenna operating range (57 GHz to 64 GHz). The dimensions are listed in the Table IV.

### B. Design of the Patch to Terminate the LWA

Since, only one port of the LWA is used for scanning the space, the second port of the LWA is terminated with a matched patch to avoid the use of second connector, that would increase the dimension of the antenna and increase the complexity of the measurement setup in the anechoic chamber (inset figure in Fig. 10). The dimensions for the patch are listed in the Table IV. The S-parameters for the patch are shown in the Fig. 9b.

### C. Performance of the Designed Prototype

1) *In Planar conditions*: The designed antenna is prototyped and the compact antenna test range (CATR) measurements are performed at the CAMILLE facilities of IETR. A photo of the prototyped LWA and the measurement setup are shown in Fig. 9c and Fig. 10 respectively. The length of the prototyped LWA is  $5.77\lambda_d$  ( $\lambda_d$  is wavelength in free space at  $f_d$ ). The  $S_{11}$  is shown in Fig.11 (a) indicating that the antenna with the feed remains well matched in the band of operation. As mentioned earlier, the LWA is designed to

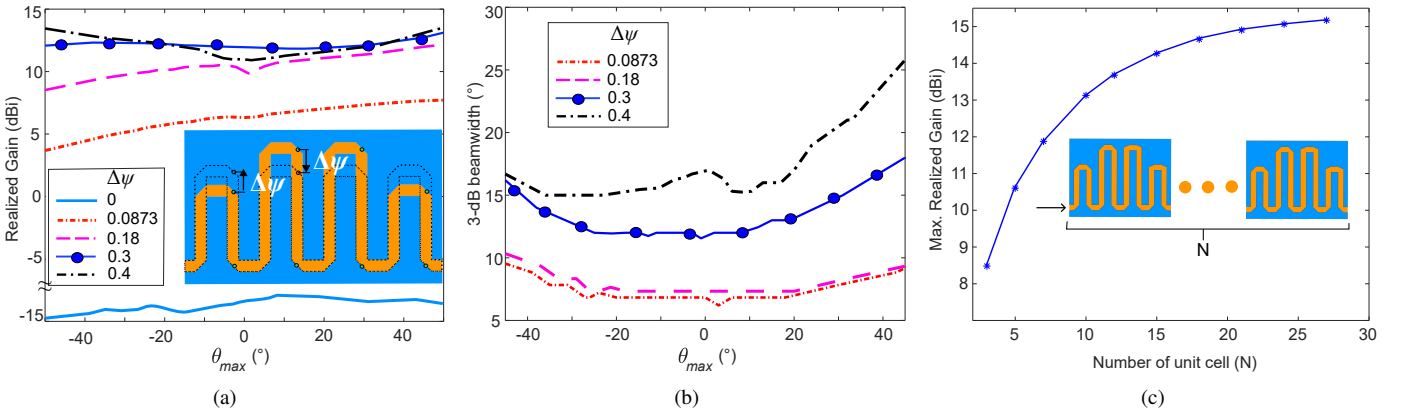


Fig. 8: (a) Maximum realized gain following the removal of the OSB in the H-plane ( $\phi = \pi/2$ ) for different  $\Delta\psi$  as a function of the beam pointing direction, (b) 3-dB beamwidth of scanning beam vs frequency for different values of  $\Delta\psi$  at  $f_d$ . (c) Maximum broadside realized gain at  $f_d$  as a function of the number of unit cells for  $\Delta\psi = 0.3$  and  $\zeta = \pi/15$ .

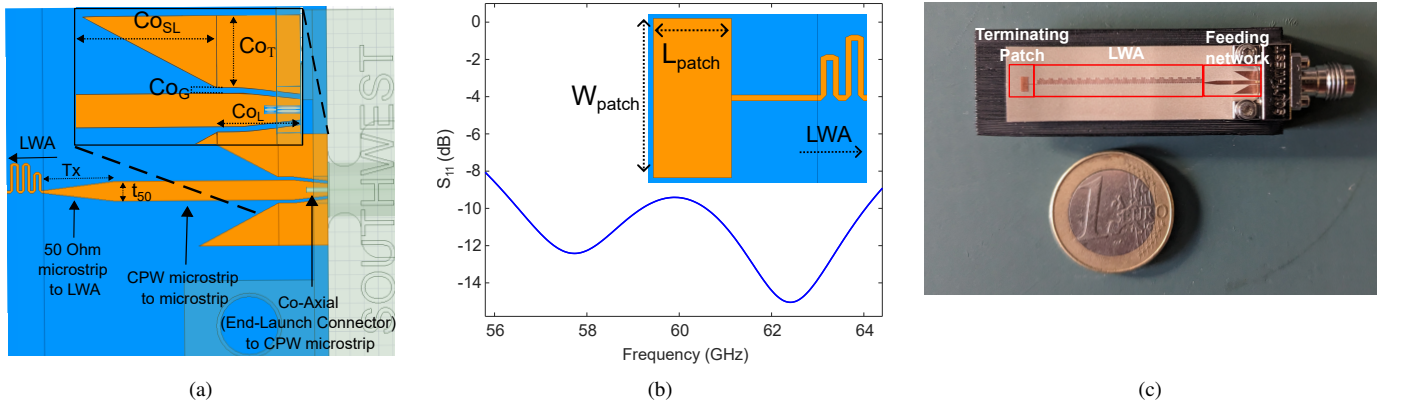


Fig. 9: (a) Design of the antenna feed. (b) Design of the patch to terminate the LWA. (c) Fabricated prototype of the LWA.

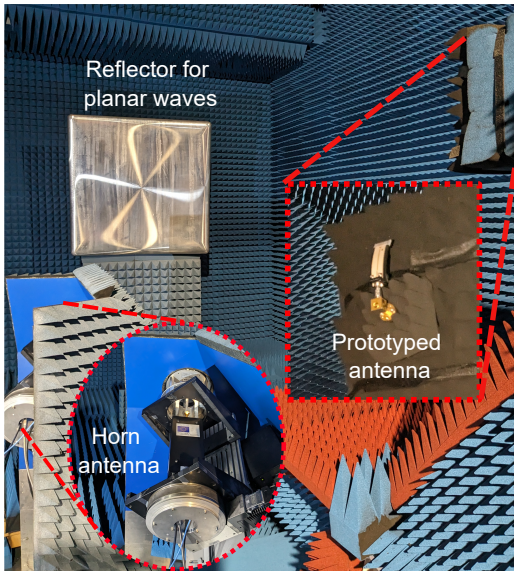


Fig. 10: CATR measurement setup for the prototype.

be linearly polarized. This can be observed in the radiation pattern in Fig.11(b–e). The LWA scans from  $-40^\circ$  to  $43^\circ$  in the range 57–64 GHz. The 3-dB beamwidth throughout the operational band remains below  $20^\circ$ . The maximum side-lobe

level remains below 10dB throughout the operational band.

The scanning rate ( $S_m$ ) of the LWA is  $12.1^\circ/\text{GHz}$ . The realized gain of the antenna stays above 10dB across the operational range as shown in the Fig. 11(f).

2) *In Conformal Conditions:* The performance of the antenna in the bent condition is investigated corresponding to the conformal placement on the knee (for  $R = 80$  mm) as shown in the Fig. 1 (b). The corresponding  $|S_{11}|$  is plotted in Fig. 12 (a) indicating the antenna remains well matched. The normalized realized gain is reported in Fig. 12(b–e). The beam-forming operation remains intact throughout the operational band for a radius of curvature  $R > 80$  mm (lower radii are not investigated currently). The realized gain decreases up to 1.5 dB when the  $R = 80$  mm as shown in Fig.12 (f).

The 3-dB beamwidth varies from  $15^\circ$  to  $23^\circ$  as depicted in Fig. 12 (f). Additionally, there is a shift in the angular scanning domain in bent condition of the LWA when compared to the planar condition [47] as shown in the Fig. 13 (a–b). The change is less than  $8^\circ$  across the band of operation.

The radiation and total efficiency of the proposed LWA are shown in Fig. 13c varying from  $-3.3$  dB to  $-2$  dB.

#### D. Enabling 2-D Scanning using Array of LWAs

An LWA, as shown in Fig. 1(b), radiates a beam enabling scanning in the X–Z plane. If 2-D scanning with a pencil beam



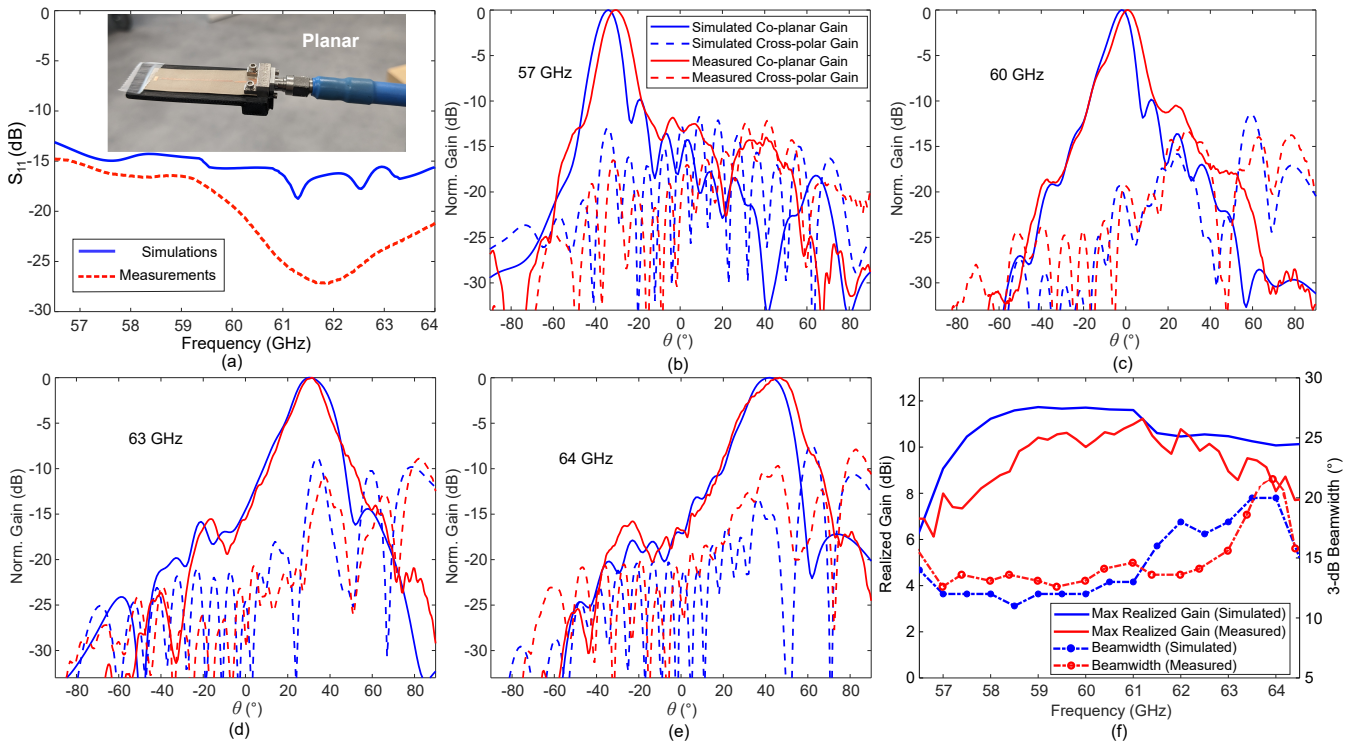


Fig. 11: (a) Simulated and Measured S parameters for the planar condition. Co-polar realized gain in the H-plane for frequencies  $f =$  (b) 57 GHz (c) 60 GHz (d) 62 GHz (e) 64 GHz (f) Simulated and measured realized gain and beamwidth for planar conditions.

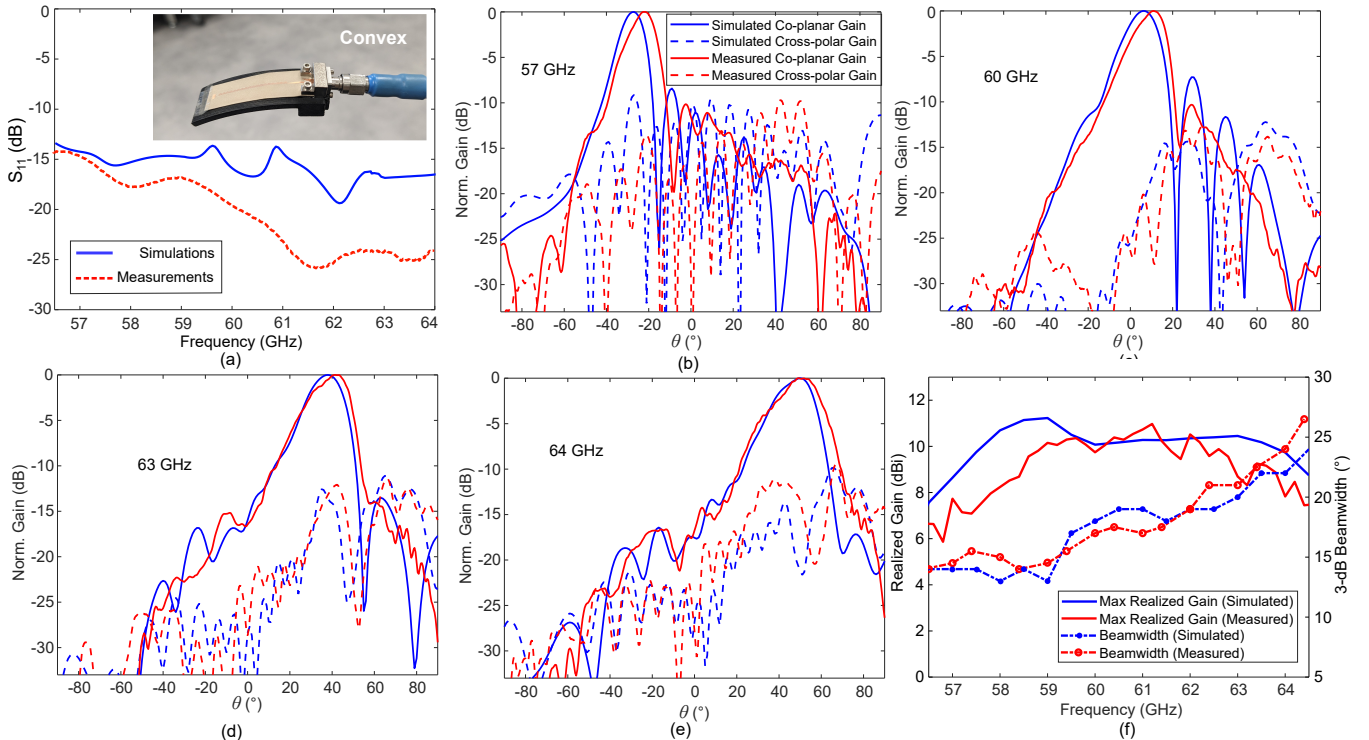


Fig. 12: (a) Simulated and measured S parameters for the bent condition with radius of curvature  $R = 80$  mm. Co-polar realized gain in the H-plane for frequencies  $f =$  (b) 57 GHz (c) 60 GHz (d) 63 GHz (e) 64 GHz (f) Simulated and measured realized gain and beamwidth for convex conditions.

is required [Fig.1 (a)], an array of LWAs using beam-forming phased excitation can be employed.

Fig.14 (a) shows the design of an array of 12 LWAs which can be implemented on a printed circuit board (PCB). This

arrangement enables a pencil-beam scanning in the X-Z and Y-Z planes as shown in Fig.14 (b). The arrangement starts by creating a pair of LWA; mirrored and excited with a phase difference of  $\pi$ . Six repetitions of such a configuration are

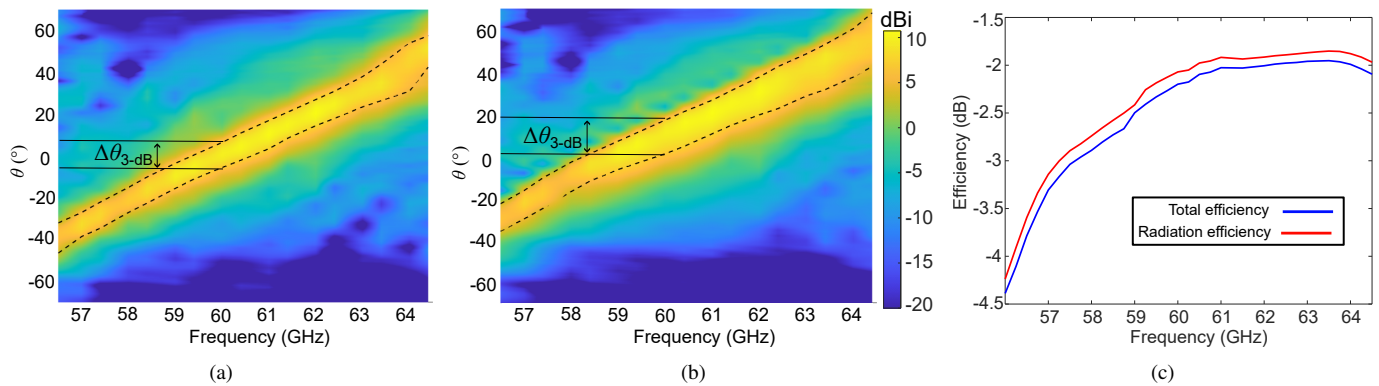


Fig. 13: Variation of the realized gain as a function of frequency for (a) planar, and (b) convex bent condition obtained from measurements. The dotted line indicates the 3-dB beamwidth. (c) Radiation and total efficiency of the proposed antenna.

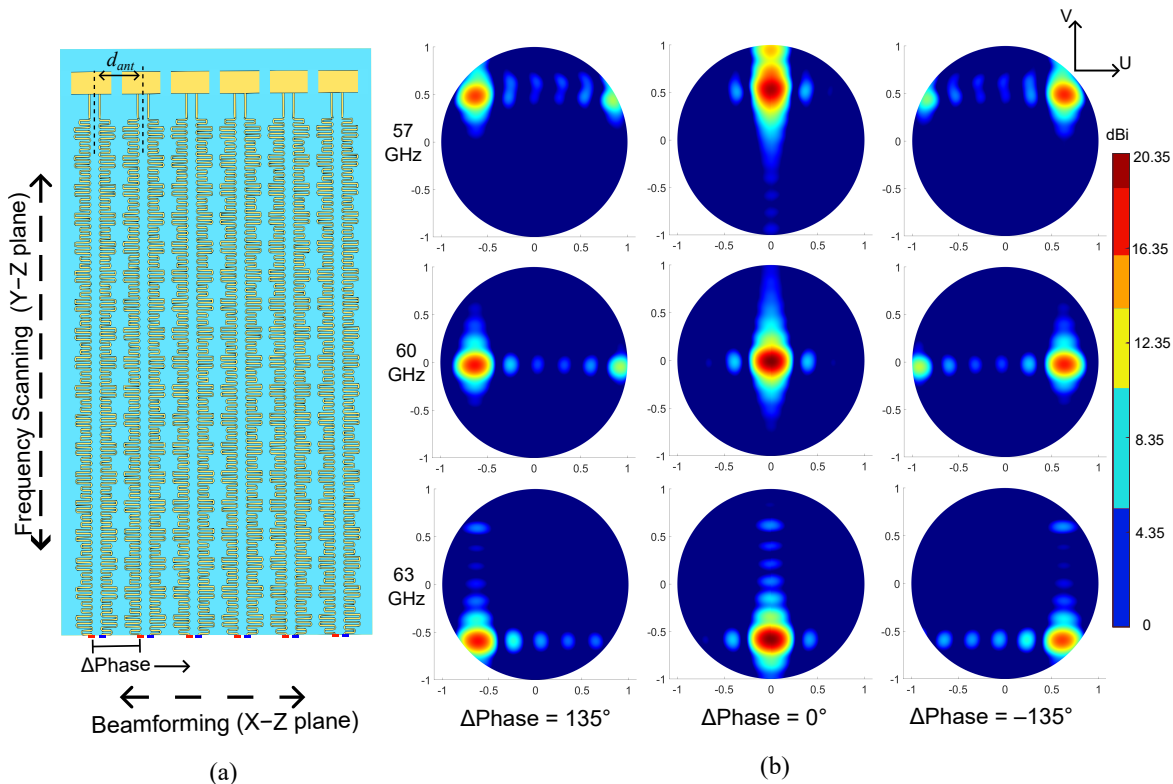


Fig. 14: (a) Array of 12 LWAs for pencil beam scanning. (b) U-V plane of the normalized realized gain showing the scanning in 2-D.

placed at a distance  $d_{\text{ant}} = 3$  mm. The phase difference between each pair can be varied to obtain beamforming in the X-Y plane.

The realized gain radiation pattern for different frequencies and phase excitations is plotted in the Fig. 14 (b) projected in the U-V plane ( $U = \sin \theta \cos \phi$ ,  $V = \sin \theta \sin \phi$ ).

Additional analysis such as the relative distance between the LWAs and phased excitation between the subsequent LWAs for planar or conformal conditions can be performed as carried out in [48].

#### E. Comparison with Other LWA Designs in V-band

In [49-51], the authors propose a frequency scanning LWA based on SIW technology. However, the  $S_m$  is limited to 2.15°/GHz, 4.45°/GHz and 8.77°/GHz respectively. LWAs

proposed in the works [52], [53] demonstrate higher or comparable scanning rate than the one proposed in this work, however, these antennas do not offer control over the scanning rate and the realized gain at the same time. A guiding medium created using the meander shaped SIW is proposed in [5], [24] to provide additional control over scanning rate, however the angular coverage is limited to 65° over the 57–64 GHz. Conformal analysis has been performed in the work [54] but the scanning occurs over a large frequency range spanning 28–62 GHz. Additionally, these LWAs utilize SIW or multi-layer guiding structures, increasing the fabrication complexity.

#### V. CONCLUSION

A single-layer low-profile V-band LWA is designed and prototyped for on-body radar applications. To allow for bending,

the antenna is designed on a flexible substrate (Rogers 3003). The proposed meandering microstrip structure allows for an accurate control the of scanning rate and realized gain. The meandering microstrip design is fast scanning and avoids the use of vias to increase the flexibility and reduce manufacturing defects and costs. Investigation of the performance of the antenna is carried out for different conformal environments. The results suggest that the beam-forming operation of the LWA remains intact even when placed on conformal surfaces although the peak realized gain reduces by 1.5 dB. Furthermore, the antenna design based on meandering microstrip can easily be integrated with a PCB. Future work involves the integration of the designed antenna with the commercially available hardware to realize an on-body radar.

#### ACKNOWLEDGMENT

The authors would like to express their gratitude to Zvonimir Šipuš for his advice on the manuscript and for sharing his insights on periodic structures and stop bands, and to Christos Monochristou for his technical insights into leaky-wave antennas and periodic structures.

#### REFERENCES

- [1] E. Cardillo, C. Li, and A. Caddemi, "Millimeter-wave radar cane: A blind people aid with moving human recognition capabilities," *IEEE J. Electromagn. RF Microw. Med. Biol.*, vol. 6, no. 2, pp. 204–211, Jun. 2022.
- [2] T. Kurata, M. Kourogi, T. Ishikawa, Y. Kameda, K. Aoki, and J. Ishikawa, "Indoor-outdoor navigation system for visually-impaired pedestrians: Preliminary evaluation of position measurement and obstacle display," in *Proc. 15th Annual International Symposium on Wearable Computers*, Jun. 2011, pp. 123–124.
- [3] N. Mahmud, R. Saha, R. Zafar, M. Bhuiyan, and S. Sarwar, "Vibration and voice operated navigation system for visually impaired person," in *Proc. International Conference on Informatics, Electronics & Vision (ICIEV)*, May 2014, pp. 1–5.
- [4] M. M. Islam, M. Sheikh Sadi, K. Z. Zamli, and M. M. Ahmed, "Developing walking assistants for visually impaired people: A review," *IEEE Sensors J.*, vol. 19, no. 8, pp. 2814–2828, Apr. 2019.
- [5] A. Shoykhetbrod, A. Hommes, and N. Pohl, "A scanning FMCW-radar system for the detection of fast moving objects," in *Proc. International Radar Conference*, Oct. 2014, pp. 1–5.
- [6] S. Bhatlawande, M. Mahadevappa, J. Mukherjee, M. Biswas, D. Das, and S. Gupta, "Design, development, and clinical evaluation of the electronic mobility cane for vision rehabilitation," *IEEE Trans. Neural Syst. Rehabil. Eng.*, vol. 22, no. 6, pp. 1148–1159, Nov. 2014.
- [7] P. Kwiatkowski, T. Jaeschke, D. Starke, L. Piotrowsky, H. Deis, and N. Pohl, "A concept study for a radar-based navigation device with sector scan antenna for visually impaired people," in *Proc. IEEE MTT-S Int. Microwave Bio Conference (IMBioC)*. Gothenburg, Sweden: IEEE, May 2017, pp. 1–4.
- [8] S. L. Cotton, W. G. Scanlon, and P. S. Hall, "A simulated study of co-channel inter-BAN interference at 2.45 GHz and 60 GHz," in *The 3rd European Wireless Technology Conference*, Sep. 2010, pp. 61–64.
- [9] Y. Rahmat-Samii and L. Song, "Advances in communication and biomedical antenna developments at the UCLA Antenna Lab: Handheld, wearable, ingestible, and implantable bioelectromagnetics," *IEEE Antennas Propag. Mag.*, vol. 63, no. 5, pp. 102–115, Oct. 2021.
- [10] A. Oliner and A. Hessel, "Guided waves on sinusoidally-modulated reactance surfaces," *IRE Trans. Antennas Propag.*, vol. 7, no. 5, pp. 201–208, Dec. 1959.
- [11] D. Zheng, C. H. Chan, and K. Wu, "Leaky-wave structures and techniques for integrated front-end antenna systems," *IEEE j. microw.*, vol. 3, no. 1, pp. 368–397, Jan. 2023.
- [12] C. A. Balanis, *Antenna Theory: Analysis and Design*. John Wiley & Sons, Dec. 2015.
- [13] P. J. Soh, G. A. Vandenbosch, M. Mercuri, and D. M.-P. Schreurs, "Wearable wireless health monitoring: Current developments, challenges, and future trends," *IEEE Microw. Mag.*, vol. 16, no. 4, pp. 55–70, May 2015.
- [14] L. Song and Y. Rahmat-Samii, "A systematic investigation of rectangular patch antenna bending effects for wearable applications," *IEEE Trans. on Antennas and Propagation*, vol. 66, no. 5, pp. 2219–2228, May 2018.
- [15] P. Vadher, G. Sacco, and D. Nikolayev, "Meandering microstrip leaky wave antenna with dual-band linear–circular polarization and suppressed open stopband," *IEEE Trans. Antennas Propag.*, vol. 72, no. 1, pp. 375–386, Jan. 2024.
- [16] —, "On-body V-band leaky-wave antenna for navigation and safety applications," in *IEEE Microwaves, Antennas, and Propag. Conf. (MAP-Con 2022)*, Bangalore, Dec. 2022, pp. 1741–1746.
- [17] P. Vadher, D. G. Sacco, and D. D. Nikolayev, "Higher spatial harmonic leaky wave antenna design based on meandering microstrips," in *Proc. 17th Eur. Conf Antennas and Propag. (EuCAP 2023)*, Florence, Italy, Mar. 2023.
- [18] S. Cheng, Y. Li, Z. Liang, S. Zheng, and Y. Long, "An approximate circuit model to analyze microstrip rampart line in osb suppressing," *IEEE Access*, vol. 7, pp. 90412–90417, 2019.
- [19] A. Sarkar, A. Sharma, A. Biswas, and M. J. Akhtar, "Compact CRLH leaky-wave antenna using TE<sub>20</sub>-mode substrate-integrated waveguide for broad space radiation coverage," *IEEE Trans. Antennas Propag.*, vol. 68, no. 10, pp. 7202–7207, Oct. 2020.
- [20] C. Caloz, T. Itoh, and A. Rennings, "CRLH metamaterial leaky-wave and resonant antennas," *IEEE Antennas Propag. Mag.*, vol. 50, no. 5, pp. 25–39, Oct. 2008.
- [21] J. Liu, X. Tang, Y. Li, and Y. Long, "Substrate integrated waveguide leaky-wave antenna with H-shaped slots," *IEEE Trans. Antennas Propag.*, vol. 60, no. 8, p. 6, May 2012.
- [22] C. Wood, "Curved microstrip lines as compact wideband circularly polarised antennas," *IEE J. Microw. Opt. Acoust. UK*, vol. 3, no. 1, p. 5, 1979.
- [23] P. Hall, "Microstrip linear array with polarisation control," *IEE Proc. H Microw. Opt. Antennas UK*, vol. 130, no. 3, p. 215, 1983.
- [24] A. Shoykhetbrod, D. Nussler, and A. Hommes, "Design of a SIW meander antenna for 60 GHz applications," in *2012 The 7th German Microwave Conference*, Mar. 2012, pp. 1–3.
- [25] G. Sacco, M. Mercuri, R. Hornung, H. Visser, I. Lorato, S. Pisa, and G. Dolmans, "A SISO FMCW radar based on inherently frequency scanning antennas for 2-D indoor tracking of multiple subjects," *Sci Rep*, vol. 13, no. 1, p. 16701, Oct. 2023.
- [26] M. Mercuri, G. Sacco, R. Hornung, P. Zhang, H. J. Visser, M. Hijdra, Y.-H. Liu, S. Pisa, B. van Liempd, and T. Torfs, "2-D localization, angular separation and vital signs monitoring using a SISO FMCW radar for smart long-term health monitoring environments," *IEEE Internet Things J.*, vol. 8, no. 14, pp. 11065–11077, Jul. 2021.
- [27] H.-H. Zhang, R. Li, J. Ren, X. Du, C. Zhang, X.-Y. Sun, Y. Yin, and M. Shen, "High-scanning-rate and wide-scanning-angle leaky-wave antenna based on double-Layer slow-wave structure," *IEEE Antennas Wireless Propag.*, vol. 22, no. 9, pp. 2145–2149, Sep. 2023.
- [28] J. L. Gómez-Tornero, "Smart leaky-wave antennas for iridescent IoT wireless networks," in *Antenna and Array Technologies for Future Wireless Ecosystems*. John Wiley & Sons, Ltd, 2022, pp. 119–181.
- [29] A. Orth, P. Kwiatkowski, and N. Pohl, "A novel approach for a MIMO FMCW radar system with frequency steered antennas for 3D target localization," in *2019 16th European Radar Conference (EuRAD)*, Oct. 2019, pp. 37–40.
- [30] P. Kwiatkowski, A. Orth, and N. Pohl, "Combining 77–81 GHz MIMO FMCW radar with frequency-steered antennas: A case study for 3D target localization," *INT J MICROW WIREL T*, pp. 1–9, Mar. 2024.
- [31] D. R. Jackson, C. Caloz, and T. Itoh, "Leaky-Wave Antennas," *Proceedings of the IEEE*, vol. 100, pp. 2194–2206, 2011.
- [32] R. E. Collin and F. J. Zucker, *Antenna Theory Part 2*. New York: McGraw-Hill, 1969, vol. 2.
- [33] A. Ishimaru, *Electromagnetic Wave Propagation, Radiation, and Scattering: From Fundamentals to Applications*, 2nd ed., ser. The IEEE Press Series on Electromagnetic Wave Theory. Piscataway, NJ: IEEE Press/Wiley, 2017.
- [34] M. R. Rahimi, M. S. Sharawi, and K. Wu, "Higher-order space harmonics in substrate integrated waveguide leaky-wave antennas," *IEEE Trans. Antennas Propag.*, vol. 69, no. 8, pp. 4332–4346, Aug. 2021.
- [35] A. Harvey, "Periodic and guiding structures at microwave frequencies," *IEEE Trans. Microwave Theory Techn.*, vol. 8, no. 1, pp. 30–61, Jan. 1960.

- [36] X. Tian, Q. Zeng, D. Nikolayev, and J. S. Ho, "Conformal propagation and near-omnidirectional radiation with surface plasmonic clothing," *IEEE Trans. Antennas Propag.*, vol. 68, no. 11, pp. 7309–7319, Nov. 2020.
- [37] R. Harrington, "Fundamental concepts," in *Time-Harmonic Electromagnetic Fields*, ser. IEEE Press Series on Electromagnetic Wave Theory. Wiley-IEEE Press, 2001, p. 36.
- [38] J. R. James and G. J. Wilson, "Microstrip antennas and arrays. Pt. 1 - Fundamental action and limitations," vol. 1, no. 5, 1977.
- [39] G. Sacco, O. Caytan, S. Pisa, and H. J. Visser, "Analysis and modelling of rampart line antennas," *IET Microw. Antennas Propag.*, vol. 15, no. 12, pp. 1605–1617, 2021.
- [40] J. R. James, P. S. Hall, and C. Wood, *Microstrip Antenna: Theory and Design*, ser. (IEE Electromagnetic Waves Series, No.12). London: IET ch 7, sec 7.4.1, pp. 215–218, 1986.
- [41] J. D. Jackson, *Classical Electrodynamics*. American Association of Physics Teachers, 1999.
- [42] C. Caloz and T. Itoh, *Electromagnetic Metamaterials: Transmission Line Theory and Microwave Applications: The Engineering Approach*. Hoboken, NJ, USA: John Wiley & Sons, Inc., 2005, Nov. 2005.
- [43] D. M. Pozar, *Microwave Engineering*, 4th ed. Hoboken, NJ: Wiley, Nov. 2011.
- [44] H. Wang, S. Sun, and X. Xue, "A periodic meandering microstrip line leaky-wave antenna with consistent gain and wide-angle beam scanning," *Int. J. RF Microw. Comput.-Aided Eng.*, vol. 32, no. 7, p. e23162, 2022.
- [45] S. Otto, A. Al-Bassam, A. Rennings, K. Solbach, and C. Caloz, "Transversal asymmetry in periodic leaky-wave antennas for bloch impedance and radiation efficiency equalization through broadside," *IEEE Trans. Antennas Propag.*, vol. 62, no. 10, pp. 5037–5054, Oct. 2014.
- [46] S.-T. Yang and H. Ling, "Application of a microstrip leaky wave antenna for range–azimuth tracking of humans," *IEEE Geosci. Remote Sensing Lett.*, vol. 10, no. 6, pp. 1384–1388, Nov. 2013.
- [47] A. J. Martinez-Ros, J. L. Gómez-Tornero, and G. Goussetis, "Conformal tapered substrate integrated waveguide leaky-wave antenna," *IEEE Trans. Antennas Propag.*, vol. 62, no. 12, pp. 5983–5991, Dec. 2014.
- [48] I. V. Soares, P. Vadher, A. K. Skrivervik, G. Sacco, and D. Nikolayev, "Analysis of non-canonical body-conformal arrays with polarization decomposition," in *Proc. 17th Eur. Conf Antennas and Propag. (EuCAP 2023)*, Florence, Italy, Mar. 2023.
- [49] M. Steeg, B. Khani, V. Rymanov, and A. Stöhr, "Novel 50–70 GHz compact PCB leaky-wave antenna with high broadside efficiency and low return loss," in *2016 41st International Conference on Infrared, Millimeter, and Terahertz Waves*, Sept. 2016, Sep. 2016, pp. 1–2.
- [50] Y. Torabi, H. Oraizi, A. Araghi, and M. Khalily, "Miniaturized V-band circularly polarized leaky-wave antenna with continuous radiation coverage using modified waveguide and metasurface CSRRs," *Sci Rep*, vol. 13, no. 1, p. 10162, Jun. 2023.
- [51] K. Neophytou, S. Iezekiel, M. Steeg, and A. Stöhr, "Design of PCB leaky-wave antennas for Wide angle beam steering," in *2018 11th German Microwave Conference (GeMiC)*, Mar. 2018, pp. 152–155.
- [52] L. Chang, Z. Zhang, Y. Li, S. Wang, and Z. Feng, "60-GHz air substrate leaky-wave antenna based on MEMS micromachining technology," *IEEE Trans. Compon. Packag. Manuf. Technol.*, vol. 6, no. 11, pp. 1656–1662, Nov. 2016.
- [53] A. Sarkar and S. Lim, "60 GHz compact larger beam scanning range PCB leaky-wave antenna using HMSIW for millimeter-wave applications," *IEEE Trans. Antennas Propagat.*, vol. 68, no. 8, pp. 5816–5826, Aug. 2020.
- [54] E. Celenk and N. Turker Tokan, "Frequency scanning conformal sensor based on SIW metamaterial antenna," *IEEE Sensors J.*, vol. 21, no. 14, pp. 16 015–16 023, Jul. 2021.